

COMPLETE IONISATION OF THE NEUTRAL GAS: WHY THERE ARE SO FEW DETECTIONS OF 21-CM HYDROGEN IN HIGH REDSHIFT RADIO GALAXIES AND QUASARS

S. J. CURRAN

Sydney Institute for Astronomy, School of Physics, The University of Sydney, NSW 2006, Australia and
ARC Centre of Excellence for All-sky Astrophysics (CAASTRO)

AND

M. T. WHITING

CSIRO Astronomy and Space Science, PO Box 76, Epping NSW 1710, Australia

Draft version June 18, 2018

ABSTRACT

From the first published $z \gtrsim 3$ survey of 21-cm absorption within the hosts of radio galaxies and quasars, Curran et al. (2008b) found an apparent dearth of cool neutral gas at high redshift. From a detailed analysis of the photometry, each object is found to have a $\lambda = 1216 \text{ \AA}$ continuum luminosity in excess of $L_{1216} \sim 10^{23} \text{ W Hz}^{-1}$, a critical value above which 21-cm has never been detected at any redshift. At these wavelengths, and below, hydrogen is excited above the ground state so that it cannot absorb in 21-cm. In order to apply the equation of photoionisation equilibrium, we demonstrate that this critical value also applies to the ionising ($\lambda \leq 912 \text{ \AA}$) radiation. We use this to show, for a variety of gas density distributions, that upon placing a quasar within a galaxy of gas there is *always* an ultra-violet luminosity above which all of the large-scale atomic gas is ionised. While in this state the hydrogen cannot be detected nor engage in star formation. Applying the mean ionising photon rate of all of the sources searched, we find, using canonical values for the gas density and recombination rate coefficient, that the observed critical luminosity gives a scale-length (3 kpc) similar that of the neutral hydrogen (H I) in the Milky Way, a large spiral galaxy. Thus, this simple, yet physically motivated, model can explain the critical luminosity ($L_{912} \sim L_{1216} \sim 10^{23} \text{ W Hz}^{-1}$), above which neutral gas is not detected. This indicates that the non-detection of 21-cm absorption is not due to the sensitivity limits of current radio telescopes, but rather that the lines-of-sight to the quasars, and probably the bulk of the host galaxies, are devoid of neutral gas.

Subject headings: galaxies: active — galaxies: ISM — radio lines: galaxies — ultra violet: galaxies — galaxies: high redshift — cosmology: early universe

1. INTRODUCTION

Hydrogen gas accounts for 75% of all the baryonic matter in the Universe, of which the cool component, the reservoir for star formation, is traced by the radio-band 21-cm spin-flip transition. Due to the low probability of the transition, compounded by the inverse square law, this is essentially undetectable at $z \gtrsim 0.2$ (see Catinella et al. 2008), although in absorption the line strength is dependent only upon the column density of the absorbing gas and the radio flux of the background source.

Hydrogen has been detected in the ultra-violet band Lyman- α transition, which traces all of the neutral gas, in 1500 high redshift galaxies *intervening* the sight-lines to more distant quasi-stellar objects (QSOs, see Curran et al. 2002; Noterdaeme et al. 2009). However, despite four decades of searches, knowledge of the cool component of this gas in the distant ($z \gtrsim 0.1$) Universe remains very scarce, with only 42 cases reported in these absorbers, *intervening* radio-loud QSOs (quasars)¹, in addition to 35 *associated* with the quasar host galaxy itself.²

sjc@physics.usyd.edu.au

¹ Compiled in Curran (2010), with the addition of those recently reported by Srikanth et al. (2010); Curran et al. (2011c).

² Compiled in Curran & Whiting (2010), with the addition of three new associated absorbers, two reported in Curran et al.

In both cases, the majority of detections occur at redshifts of $z \lesssim 1$ (look-back times $\leq 7.7 \text{ Gyr}$).³ In the case of the intervening absorbing galaxies, the apparent lack of cold gas at high redshift may be accounted for by geometry effects: In an expanding Universe absorbers at redshifts of $z \gtrsim 1$ are *always* disadvantaged, in comparison to the low redshift ($z \lesssim 1$) absorbing galaxies, in how effectively the absorber can cover the higher redshift background source (Curran & Webb 2006; Curran 2012).

Since for the associated systems the absorbing gas is located within the quasar host galaxy, such geometry effects cannot account for the fact that the 21-cm detection rate at $z \lesssim 1$ is double that at $z \gtrsim 1$. Furthermore, only one associated 21-cm absorber has ever been found at $z > 3$ (Uson et al. 1991). This runs contrary to the expectation that at these redshifts (look-back times $\geq 11.5 \text{ Gyr}$), much of the gas has yet to be consumed by star formation, meaning that we would expect the abundance of hydrogen to be many times higher than in the present day Universe (e.g. Péroux et al. 2001).

In addition to these covering factor effects, for a given column density, the optical depth of the 21-cm absorp-

(2011a) and one in Curran et al. (2011d). See also Allison et al. (2012).

³ We employ a standard Λ cosmology with $H_0 = 71 \text{ km s}^{-1} \text{ Mpc}^{-1}$, $\Omega_{\text{matter}} = 0.27$ and $\Omega_{\Lambda} = 0.73$.

tion is dependent upon the spin temperature of the gas (Wolfe & Burbidge 1975). Since only atoms populating the lower hyperfine level can absorb in 21-cm, the spin temperature may be elevated through:

1. Excitation to the upper hyperfine level (Purcell & Field 1956).
2. Excitation above the ground state, particularly by Lyman- α ($\lambda = 1216 \text{ \AA}$) photons (Field 1959).
3. Ionisation.

Although, with the data available, excitation to the upper hyperfine level through collisions (Purcell & Field 1956, see also Draine 2011) cannot be ruled out, Curran et al. (2008b) find no dependence of the 21-cm detection rate on the rest-frame 1420 MHz continuum luminosity of the active galactic nucleus (AGN), thus at least ruling out excitation through this radiative process.

Curran et al. (2008b) do, however, find a strong dependence on the rest-frame $\lambda = 1216 \text{ \AA}$ ($\nu = 2.47 \times 10^{15} \text{ Hz}$) continuum luminosity. Specifically, that 21-cm absorption has *never* been detected above an apparent critical luminosity of $L_{1216} \sim 10^{23} \text{ W Hz}^{-1}$. For a $\approx 50\%$ detection rate at $L_{1216} \lesssim 10^{23} \text{ W Hz}^{-1}$ (Curran et al. 2008b), the probability of 0 detections out of 19 searches occurring by chance is 1.9×10^{-6} (significant at 4.76σ assuming Gaussian statistics, Curran et al. 2011a). So although the gas may be excited through other processes (collisions and the Cosmic Microwave Background), this correlation strongly suggests that excitation above the ground state (and possible ionisation) by $\lambda \leq 1216 \text{ \AA}$ photons is the dominant cause of the non-detections.

Given that 17 of the 19 $L_{1216} \geq 10^{23} \text{ W Hz}^{-1}$ sources are type-1 AGN, it is also possible that the absorption, by cool gas in the circumnuclear obscuring torus invoked by unified schemes, simply does not occur along our line-of-sight to the continuum source (e.g. Morganti et al. 2001; Pihlström et al. 2003; Gupta et al. 2006). However, at $L_{1216} \leq 10^{23} \text{ W Hz}^{-1}$, *both* type-1 and type-2 AGN exhibit a 50% detection rate (Curran et al. 2008b, 2011a), indicating the absorption must primarily arise in the main galactic disk, which is randomly oriented with respect to the torus. Therefore, the bias towards type-1 objects at $L_{1216} \gtrsim 10^{23} \text{ W Hz}^{-1}$ is due to these tending to arise in the more luminous quasars, as opposed to radio galaxies, which tend to be associated with type-2 objects and is therefore not an orientation effect (Curran & Whiting 2010).

Thus, Curran et al. (2008b) interpreted their exclusive non-detections at $z \gtrsim 3$ to the traditional optical selection of targets, in conjunction with the high redshifts, introducing a bias towards the sources more luminous in rest-frame ultra-violet.⁴ The same critical ultra-violet continuum luminosity is also evident in the lower redshift surveys (see Allison et al. 2012) and attributing the lack of cold gas in the hosts of powerful AGN to the high ultra-violet luminosities exciting the gas beyond detection (which we dub “*the UV interpretation*”), can explain

⁴ Despite shortlisting the faintest objects (with blue magnitudes of $B \gtrsim 19$, see figure 5 of Curran et al. 2009).

why this effect is seen at all redshifts. The UV interpretation may also account for several other issues in extragalactic radio astronomy, such as the elevated detection rate in compact objects and the preference for 21-cm detection in radio galaxies over quasars (Curran & Whiting 2010).

Given the low probability of zero detections occurring by chance above a given 1216 \AA continuum luminosity, in conjunction the fact that $\lambda < 1216 \text{ \AA}$ photons excite (and possibly ionise) the gas so that it cannot absorb in 21-cm, there is little doubt that the UV interpretation is the correct physical description. This has been confirmed by an independent survey for 21-cm in 143 radio sources at redshifts $0.02 < z < 3.8$, where the lack of detections is correlated with the UV luminosity (Grasha & Darling 2011), as well as by Page et al. (2012), who find a critical X-ray luminosity, above which sources are not detected in 250 μm continuum emission, a tracer of star formation.

However, one question remains unanswered: Why is there a hard limit to the UV luminosity, above which the gas is excited beyond detection by the most sensitive radio telescopes, rather than a continuum where the detections gradually become fewer and fewer as the ultra-violet luminosity increases? We address this issue here.

2. PHOTOIONISATION EQUILIBRIUM

For a cloud of hydrogen containing an ionising source, the equilibrium between photoionisation and recombination of protons and electrons in a nebula can be written as (Osterbrock 1989),

$$\int_{\nu_{\text{ion}}}^{\infty} \frac{L_{\nu}}{h\nu} d\nu = 4\pi \int_0^{r_{\text{ion}}} n_{\text{p}} n_{\text{e}} \alpha_{A,B} r^2 dr, \quad (1)$$

where L_{ν} is the specific luminosity at frequency ν and h is the Planck constant, giving the number of ionising photons per second. On the right hand side, r_{ion} is the extent of the ionisation, n_{p} and n_{e} are the proton and electron densities, respectively, and $\alpha_{A,B}$ the radiative recombination rate coefficient of hydrogen (see Sect. 2.2).

Since, after excitation to the upper hyperfine level, the next excitation is to $n = 2$ by Lyman- α photons, our proxy has been the $\lambda = 1216 \text{ \AA}$ continuum luminosity. However, since excitation to the $n = 2$ level and ionisation of the hydrogen atom are so close in energy (both events being $\approx 2 \times 10^6$ times as energetic as the spin-flip transition), this critical luminosity should also apply in the case of ionisation. In order to verify this, in Fig. 1 we show the $\lambda = 912 \text{ \AA}$ continuum luminosity distribution. The luminosities have been derived from the photometries as described in Curran et al. (2008b), but with the inclusion of data from the Galaxy Evolution Explorer (GALEX, Martin et al. 2003). These, in conjunction with the *BVRK* magnitudes from the literature, allow reliable power-law fits to the rest-frame UV data (corrected for Galactic extinction using the maps of Schlegel et al. 1998) over a range of redshifts, from which the $\lambda = 912 \text{ \AA}$ continuum luminosities were derived (see Curran et al. 2012).

From Fig. 1, we see that the same approximate critical value applies in the case of ionising photons. That is, 21-cm absorption has never been detected above a luminosity close to $L_{912} \sim 10^{23} \text{ W Hz}^{-1}$. The largest

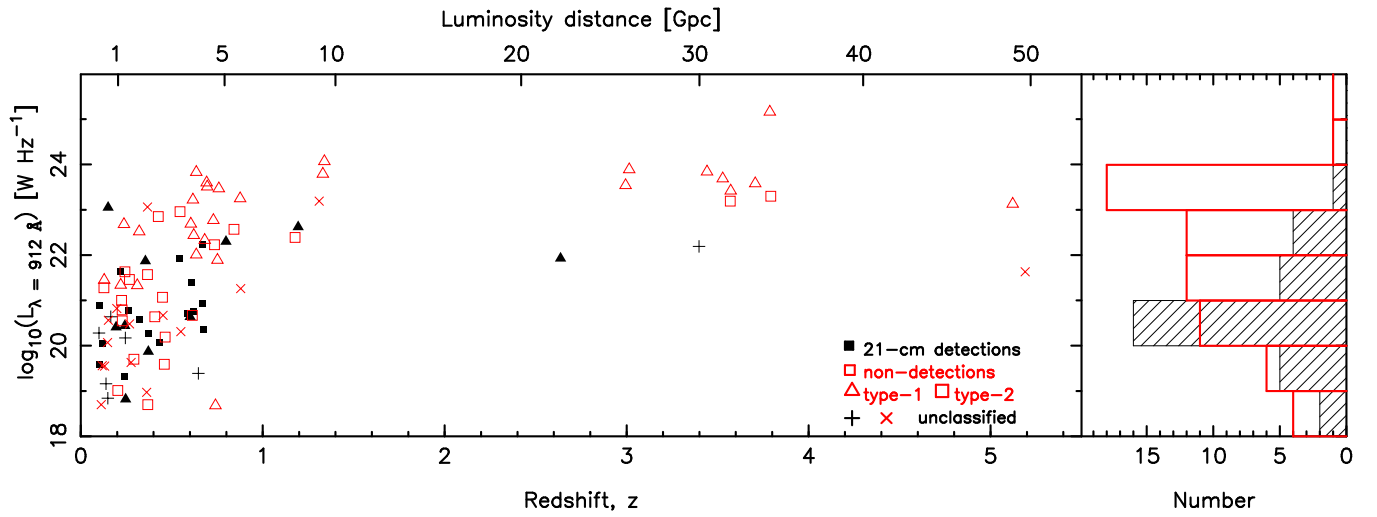


FIG. 1.— The $\lambda = 912 \text{ \AA}$ continuum luminosity (where available, see Curran et al. 2012) versus redshift for the sources searched in 21-cm absorption. The filled symbols/hatched histogram represent the 21-cm detections and the unfilled symbols/unfilled histogram the non-detections. The shapes represent the AGN classifications, with triangles representing type-1 objects and squares type-2s (+ and x designate an undetermined AGN type for a detection and non-detection, respectively).

measured 912 Å luminosity for which there is a detection is $L_{912} = 1.1 \times 10^{23} \text{ W Hz}^{-1}$, above which there are 20 non-detections. Of the sources for which we could reliably determine L_{912} , there are 38 detections and 60 non-detections (i.e. a 39% detection rate) below this luminosity. Applying this probability of $p = 0.61$ for a non-detection to the $L_{912} > 1.1 \times 10^{23} \text{ W Hz}^{-1}$ sources, there is a binomial probability of 5.09×10^{-5} of the 20 non-detections occurring by chance, a 4.05σ significance.

Thus, although only excitation above the ground state is required to explain the dearth of 21-cm absorption in UV luminous sources, it is possible that ionisation of the gas is the primary cause of the non-detections. Given that the lifetime in the $n = 2$ state is only $\sim 10^{-8}$ sec, this is the more likely situation and so we are justified in applying Eq. 1 to this problem. Thus, in Sect. 2.1 we derive the value of the left hand side of the equation, for the sources searched in 21-cm, and in Sect. 2.2, we apply various recombination models to the right hand side of the equation.

2.1. Photoionisation rates

In addition to determining the UV fluxes from the GALEX photometries and the *BVRK* magnitudes, in order to investigate differences between the 21-cm detected and UV luminous non-detected samples, we obtained multi-wavelength data from all of the relevant photometries given by the NASA/IPAC Extragalactic Database (NED), again correcting for Galactic extinction using the maps of Schlegel et al. (1998). As per the $\lambda = 912 \text{ Å}$ continuum luminosities, above, we used the redshifts of the targets to blue-shift the observed frequencies back to the source rest-frame values and converted the observed fluxes to luminosities. We then averaged all of the luminosities within a specified frequency range to obtain a composite SED for all of redshifted the sources searched in 21-cm absorption.

Performing a Kolmogorov-Smirnov test between the binned luminosities of the various sub-samples (shown in each panel of Fig. 2), we find no evidence that the 21-cm detected and $L_{UV} \lesssim 10^{23} \text{ W Hz}^{-1}$ non-detected samples are drawn from different populations, with a probability of $\gtrsim 0.2$ (for all bin widths) that they are drawn from the same population. However, between either the 21-cm detected/ $L_{UV} \lesssim 10^{23} \text{ W Hz}^{-1}$ non-detected samples and the $L_{UV} \gtrsim 10^{23} \text{ W Hz}^{-1}$ sample, it is seen that, for sufficiently high resolution bins, the probability can get as low as 1×10^{-6} , although this is due to the extra high frequency points in the $L_{UV} \lesssim 10^{23} \text{ W Hz}^{-1}$ non-detected sample, with a probability of ≈ 0.004 being more likely. This still suggests, however, that the UV luminous sources are drawn from a different sample than those with $L_{UV} \lesssim 10^{23} \text{ W Hz}^{-1}$.

In order to obtain the rate of ionising photons, we are interested in frequencies above $\nu = 3.29 \times 10^{15} \text{ Hz}$. However, as seen from Fig. 2, there is a large gap in the SEDs between $\sim 10^{16}$ and $\sim 10^{17} \text{ Hz}$, the range of spaced-based ultra-violet observations between the optical and X-ray bands. Although the X-ray observations are also space-based, these generally have more sky coverage than the ultra-violet observations and are thus more likely to have observed one of our sources. So, in order to obtain an estimate of $\int_{\nu_{\text{ion}}}^{\infty} (L_{\nu}/\nu) d\nu$, where $\nu_{\text{ion}} = 3.29 \times 10^{15} \text{ Hz}$, we

smooth the SEDs (Fig. 3) and interpolate a power-law fit between $\sim 10^{16}$ and $\sim 10^{20} \text{ Hz}$ to obtain the mean dependence of L_{ν} on ν . The photon rate is given by

$$\int_{\nu_{\text{ion}}}^{\infty} \frac{L_{\nu}}{h\nu} d\nu, \text{ where } \log_{10} L_{\nu} = \alpha \log_{10} \nu + C \Rightarrow L_{\nu} = 10^C \nu^{\alpha}$$

for a power-law, where α is the spectral index and C the intercept. Solving this,

$$\frac{10^C}{h} \int_{\nu_{\text{ion}}}^{\infty} \nu^{\alpha-1} d\nu = \frac{10^C}{\alpha h} [\nu^{\alpha}]_{\nu_{\text{ion}}}^{\infty} = \frac{-10^C}{\alpha h} \nu_{\text{ion}}^{\alpha} \text{ where } \alpha < 0.$$

From the composite SEDs, for the non-UV luminous sample we find $L_{\nu} \approx 10^{37.3} \nu^{-0.95} \text{ W Hz}^{-1}$, giving 5.5×10^{55} ionising photons sec^{-1} and for the UV luminous sample, $L_{\nu} \approx 10^{34.6} \nu^{-0.68} \text{ W Hz}^{-1}$, giving 2.9×10^{57} ionising photons sec^{-1} . This is ≈ 50 times the luminosity of the 21-cm detected sample, which is consistent with the factor of ≈ 7 in the luminosity distances between the $z \gtrsim 3$ sample and the cluster of 21-cm detections at $z \lesssim 0.9$ (Fig. 1).

2.1.1. The critical photoionisation rate

Since we are interested in the ionising photon rate resulting from a critical luminosity of $L_{UV} \sim 10^{23} \text{ W Hz}^{-1}$ (Fig. 1), we use the highest 21-cm detected luminosity of $L_{912} = 1.1 \times 10^{23} \text{ W Hz}^{-1}$ at $3.29 \times 10^{15} \text{ Hz}$, together with the above spectral index of $\alpha = -0.68$, to obtain $L_{\nu} \approx 10^{33.6} \nu^{-0.68} \text{ W Hz}^{-1}$, which gives $2.9 \times 10^{56} \text{ sec}^{-1}$ for the critical ionising photon rate. Referring to the literature, from the spectra of several hundred QSOs, Telfer et al. (2002) find a mean optical-X-ray slope of $\alpha = -1.5$. This is significantly steeper than the mean spectral index derived for our sample, which consists exclusively of powerful radio sources, although applying a critical luminosity of $L_{912} = 1.1 \times 10^{23} \text{ W Hz}^{-1}$ gives $L_{\nu} \approx 10^{46.3} \nu^{-1.5} \text{ W Hz}^{-1} \Rightarrow 1.1 \times 10^{56} \text{ sec}^{-1}$, which is in the ballpark of the value derived for our sample. This is a consequence of the steeper spectral index being compensated by a larger constant (intercept) and the fact that the lower frequency end of the UV SED ($\nu \sim 3.3 \times 10^{15} \text{ Hz}$) contains most of the energy. We are therefore confident in applying $\int_{\nu_{\text{ion}}}^{\infty} (L_{\nu}/h\nu) d\nu = 2.9 \times 10^{56}$ photons sec^{-1} to the left hand side of Eq. 1.⁵

Lastly, it is clear that, while the specific continuum luminosity (L_{1216} or L_{912}) may provide an indicator of the amount ionising radiation from the AGN, the integrated ionising luminosity (i.e. the ionising photon rate) is the correct measure. By fitting polynomials to the photometry of the individual sources (Curran et al. 2012), in Fig. 4 we re-plot Fig. 1 in terms of $\int_{\nu_{\text{ion}}}^{\infty} (L_{\nu}/h\nu) d\nu$. For those for which accurate polynomial fits could be obtained, we see that above $\sim 10^{56}$ ionising photons sec^{-1} , 21-cm searches have resulted in exclusive non-detections. The highest photon rate for a detection, which could be reliably determined, is $1.7 \times 10^{55} \text{ sec}^{-1}$, a value above which there are 29 non-detections. Below this rate there

⁵ Other studies of the UV continuum slope in quasars and AGN indicate their spectral indices to be in the range $\alpha = -1.4$ to -0.56 , although with considerable scatter. These give critical photon rates of $\sim 5 \times 10^{55}$ and $\sim 2 \times 10^{54} - 2 \times 10^{57} \text{ sec}^{-1}$ (Scott et al. 2004; Shull et al. 2012, respectively).

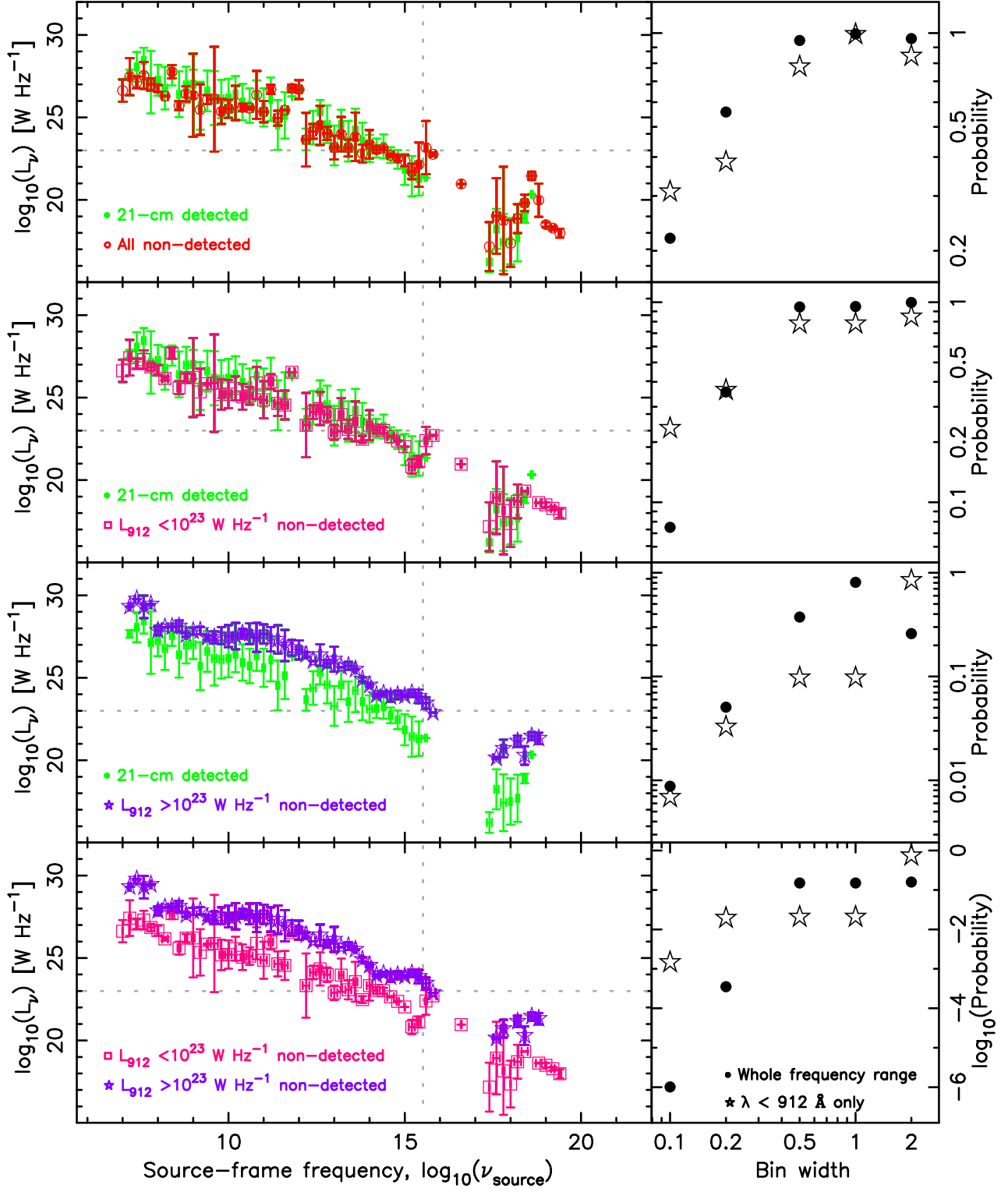


FIG. 2.— The composite SEDs for each of the various sub-samples for a bin width of ± 0.1 (i.e. each bin is $10^{2 \times 0.1} = 1.6$ times the frequency of the previous). In the left panel the vertical dotted line shows the source-frame frequency of $\nu = 3.29 \times 10^{15}$ Hz ($\lambda = 912$ Å), above which the photons ionise the atom. The right panel shows the probability, from a Kolmogorov-Smirnov test, that the two samples tested are from the same population for various bin widths for both the whole frequency range (filled circles) and $\lambda \leq 912$ Å (hollow stars).

are 38 detections and 51 non-detections, giving a $p = 0.57$ probability of a non-detection. Using this proxy, the binomial probability of 29 out of 29 non-detections occurring by chance is just 8.32×10^{-8} . This 5.36σ result therefore strongly suggests that ionisation of the gas by $\lambda \leq 912 \text{ \AA}$ photons from the AGN is responsible for the non-detection of 21-cm absorption in high redshift sources.

2.2. Recombination models

We now parametrise the right hand side of the photoionisation equilibrium expression (Eq. 1). Since we are concerned with the ionisation of neutral gas and its subsequent recombination, $n_p = n_e = n$. Also, in optical band observations of an optically thick plasma, where direct capture onto the ground state is excluded, α_B is used. However, since we are concerned with the ground state, α_A is the relevant total recombination rate coefficient (Osterbrock & Ferland 2006). We choose this value at 2000 K, $\alpha_A = 1.27 \times 10^{-12} \text{ cm}^3 \text{ sec}^{-1}$,⁶ the typical upper limit to the spin temperature found in intervening absorbers (when the Lyman- α line is also detected and an upper limit to the spin temperature can be determined, Curran et al. 2010).

Naïvely assuming a constant particle density of $n = 10 \text{ cm}^{-3}$ (typical of the cool neutral 21-cm absorbing interstellar medium) throughout the nebula, we find $r_{\text{ion}} = 3$ and 13 kpc for the mean radii of the ‘‘Strömgren spheres’’ of the UV non-luminous and UV luminous samples, respectively. Although the latter value is of the same order of magnitude as the extent of neutral gas in a large galaxy, this model represents a gradual increase in ionised radius with luminosity, with no critical value.

2.2.1. Exponential gas density distribution

Unlike the idealised ionised region around a star, we do not expect the gas density to remain constant on galactic scales. A more realistic model of the density of the cold neutral medium (CNM) within a galaxy is that of an exponential decrease in the gas density with distance from the nucleus (Begeman et al. 1991; Kalberla et al. 2007). Thus, for $n = n_0 e^{-r/R}$, where n_0 is the gas density at $r = 0$ and R is a scale-length describing the rate of decay of this with radius, Eq. 1 becomes

$$\int_{\nu_{\text{ion}}}^{\infty} \frac{L_\nu}{h\nu} d\nu = 4\pi \alpha_A n_0^2 \int_0^{r_{\text{ion}}} e^{-2r/R} r^2 dr$$

$$= \pi \alpha_A n_0^2 \left[R^3 - R e^{-2r_{\text{ion}}/R} (2r_{\text{ion}}^2 + 2r_{\text{ion}}R + R^2) \right] (2)$$

Unlike the constant density distribution, this becomes independent of r at sufficiently large radii, i.e. $\int_{\nu}^{\infty} (L_\nu/h\nu) d\nu \rightarrow \pi \alpha_A n_0^2 R^3$. Conversely, for a given scale-length, R , there *always* exists a ‘‘ceiling luminosity’’ (the number of ionising photons $\times h$) for which *all* of gas is ionised (Fig. 5).

Using the above values of $\alpha_A = 1.27 \times 10^{-12} \text{ cm}^3 \text{ sec}^{-1}$ and $n_0 = 10 \text{ cm}^{-3}$, the critical ionising photon rate of $2.9 \times 10^{56} \text{ sec}^{-1}$ gives a scale-length of $R = 2.9$ kpc. We can compare this to the H I in the Milky Way,

⁶ Compared with $\alpha_B = 0.90 \times 10^{-12} \text{ cm}^3 \text{ sec}^{-1}$, hence the choice of α_A or α_B making little difference.

where Kalberla & Kerp (2009) fit an exponential profile to the mid-plane volume density distribution to find $R = 3.15$ kpc and $n_0 = 0.9 e^{R_{\odot}/R} = 13.4 \text{ cm}^{-3}$. This is in close agreement with our values, demonstrating that the mean SED normalised by a $\lambda = 912 \text{ \AA}$ continuum luminosity of $10^{23} \text{ W Hz}^{-1}$ is sufficient to ionise all of atomic gas in a large spiral galaxy, rendering it undetectable in 21-cm.

It is therefore clear that an exponential decrease in gas density with distance from the nucleus can naturally yield a critical value in the UV luminosity which is close to that found observationally. This does however, rely on a simple model of the CNM, within which various structures and phases will be embedded, such as the warm neutral medium, as well as localised regions of ionised gas and dense molecular clouds. However, here we are modelling the large-scale CNM, for which an exponential density distribution is a realistic model (Begeman et al. 1991; Kalberla et al. 2007).

Although using the canonical values for α and n_0 gives the correct scale-length for the observed photon rate, a further physical (sanity) check can be obtained by deriving the total gas mass from the gas density and volume via $M_{\text{gas}} = \int_0^r \rho dV$. In this case, where the particle density of n protons cm^{-3} corresponds to $\rho = 1.67 \times 10^{-21} \times n \text{ kg m}^{-3}$, exponentially decaying with r across a disk of thickness, $t(r) = r/f_{\text{FL}}$, we have

$$M_{\text{gas}} = 2\pi n_0 \int_0^r e^{-r/R} r t dr = \frac{2\pi n_0}{f_{\text{FL}}} \int_0^r e^{-r/R} r^2 dr$$

$$= \frac{2\pi n_0 R^3}{f_{\text{FL}}} \left[2 - e^{-r/R} \left(\frac{r^2}{R^2} + 2\frac{r}{R} + 2 \right) \right], (3)$$

where the flare factor, f_{FL} , describes the flaring of the H I gas scale-height with galactocentric radius. Applying the mean Milky Way value of $f_{\text{FL}} \approx 20$ (Kalberla et al. 2007), a scale-length of $R = 2.9$ kpc gives a total gas mass of $M_{\text{gas}} = 7.5 \times 10^9 M_{\odot}$ (Fig. 5, bottom panel). This is close to the mean value found from a low redshift survey of 21-cm emission from the 1000 H I brightest galaxies in the southern sky (Koribalski et al. 2004), giving us further confidence in the exponential decay model and choice of gas density.

2.2.2. Alternative temperatures and disk profiles

Although spin temperatures in intervening 21-cm absorbers may be, on average, $\lesssim 2000$ K, without the total neutral hydrogen column density from the Lyman- α transition, as is the case for the associated absorbers, an upper limit to the spin temperature cannot be computed. Traditionally in the discussion of gas ionisation, temperatures of $\sim 10^4$ K are brandished (e.g. Osterbrock 1989; Haiman & Rees 2001), although these are in the case of Lyman- α emission, rather than the much less energetic 21-cm absorption. Given that the gas is most likely ionised however, in Fig. 6 (top panel) we show the ionising luminosity versus the extent of the ionised gas for $\alpha_A = 4.19 \times 10^{-13} \text{ cm}^3 \text{ sec}^{-1}$ (i.e. at 10^4 K). From the observed critical rate of $2.9 \times 10^{56} \text{ photons sec}^{-1}$, we see that the scale-length increases to $R = 4.2$ kpc, which is larger than that of the Milky Way. Thus, for this temperature the photon rate is more than that required to ionise all of the neutral gas, while demonstrating that

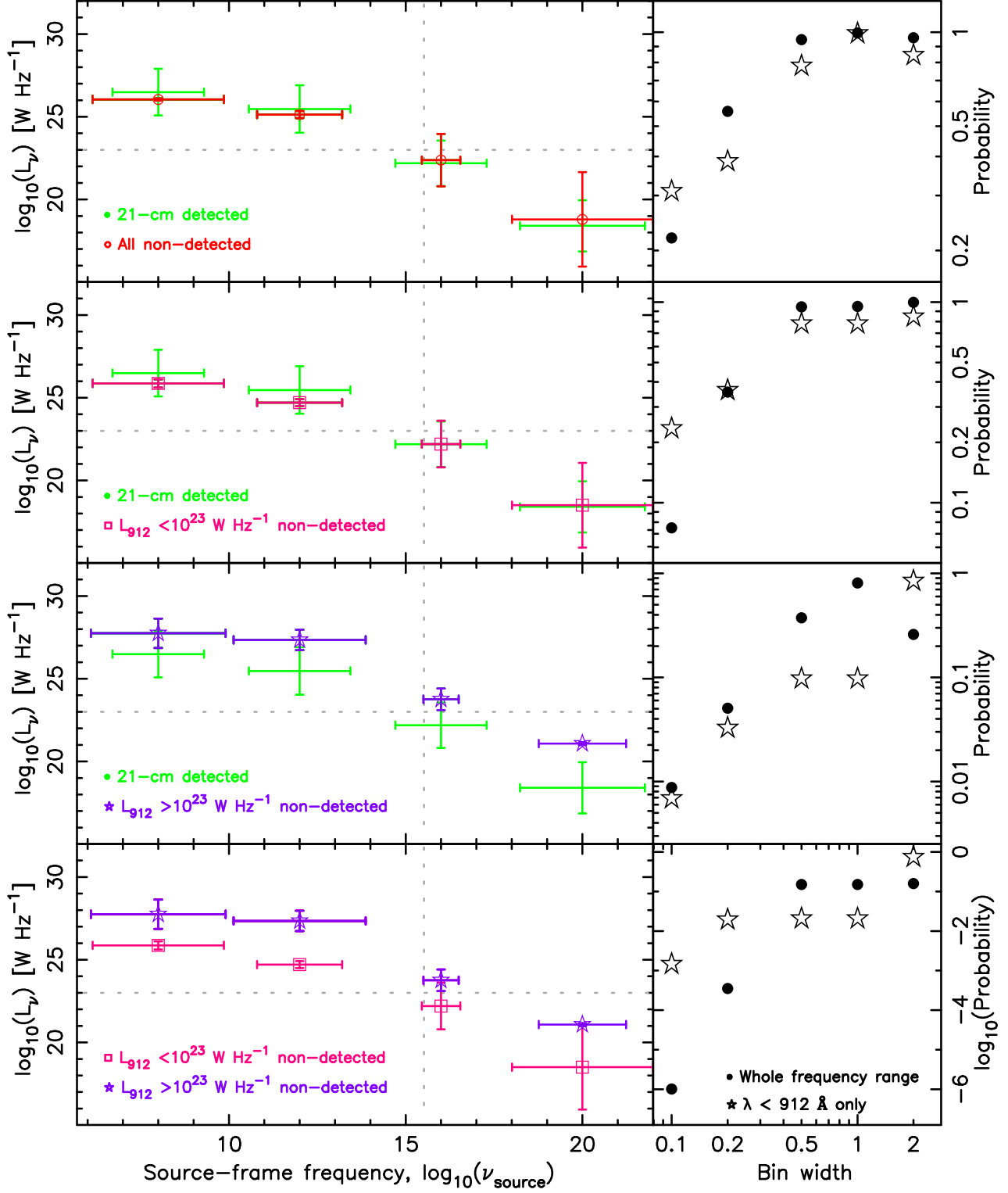


FIG. 3.— As Fig. 2 but for a bin width ± 2 (i.e. each bin is $10^{2 \times 2} = 10\,000$ times the frequency of the previous). In this and Fig. 2, the symbol shows the mean luminosity at the centre of the frequency bin (e.g. at $10^8, 10^{10}, \dots, 10^{20}$ Hz here) with the errors bars showing the standard deviation in both luminosity and frequency.

our main result is not overly sensitive to the choice of temperature.⁷

Although having no effect on the extent of the ionisation, in order to investigate the effect of a different disk profile on the mass, in Fig. 6 we show the distribution of gas mass for a sphere, rather than a disk (i.e. $dV = 4\pi r^2 dr$). For $R = 4.2$ kpc, this gives a total gas mass of $M_{\text{gas}} = 4.6 \times 10^{11} M_{\odot}$, which is close to the total (dynamical) mass expected in a galaxy and is thus too high⁸ and, applying a temperature of 2000 K (i.e. $R = 2.9$ kpc), lowers this only slightly to $M_{\text{gas}} = 1.5 \times 10^{11} M_{\odot}$. This confirms that the disk model, which reproduces a gas mass close to the typically observed value, is the more physically accurate distribution. Furthermore, although the most luminous quasars may reside in elliptical galaxies (Taylor et al. 1996), this shape traces the stellar distribution and not necessarily that of the neutral gas. For instance, “superdisks” of gas and dust in the elliptical hosts of powerful radio galaxies have been proposed (Athreya et al. 1998; Gopal-Krishna & Wiita 2000), with diameters of $\gtrsim 75$ kpc (Gopal-Krishna & Wiita 2000), perhaps up to ≈ 300 kpc (Curran et al. 2011d).

2.2.3. Alternative gas distributions

For completeness, we investigate several alternative density distributions for the gas. These are typically profiles that arise from dynamical models, often applied to the dark matter content of a galaxy, although we are interested in their effects when applied to the distribution of the CNM. The Jaffe profile (Jaffe 1983) models the distribution of light in a spherical galaxy as $n = n_0 (r_s/r)^2 / 4\pi (1 + r/r_s)^2$, where r_s is the radius which contains half the total emitted light. In this case Eq. 1 becomes

$$\begin{aligned} \int_{\nu_{\text{ion}}}^{\infty} \frac{L_{\nu}}{h\nu} d\nu &= 4\pi \alpha_A n_0^2 \int_0^{r_{\text{ion}}} \frac{r^2 (r_s/r)^4}{(4\pi)^2 (1 + r/r_s)^4} dr \\ &= -\frac{4}{3}\pi \alpha_A n_0^2 r_s^3 \left[\frac{r_s (3r_s^3 + 22r_s^2 r + 30r_s r^2 + 12r^3)}{r(r_s + r)^3} \right. \\ &\quad \left. - 12 \ln(r_s + r) + 12 \ln(r_s) \right]_0^{r_{\text{ion}}} \quad (4) \end{aligned}$$

However, due to the “cuspy” nature of the distribution, solving this over these limits yields infinities and between any reasonable limits yields unreasonably large numbers, even when the approximation $n = n_0 (r_s/r)^2 / 4\pi (1 + r/r_s)^2 \approx n_0 (r_s/r)^2 / 4\pi (r/r_s)^2 = (n_0/4\pi)(r_s/r)^4$ is used.

A similarly asymptotic density distribution is given by the Navarro–Frenk–White (NFW) profile (Navarro et al. 1996), which models the density as the distribution of dark matter in the halo, via $n = n_0 (r_c/r)/(1 + r/r_c)^2$, where n_0 and r_c are the core density and radius of the halo, respectively. Here the right hand side of Eq. 1 becomes

$$4\pi \alpha_A \int_0^{r_{\text{ion}}} n^2 r^2 = 4\pi \alpha_A n_0^2 \int_0^{r_{\text{ion}}} \frac{r^2 (r_c/r)^2}{(1 + r/r_c)^4} dr$$

⁷ Since $\alpha \propto \sqrt{T}$ (<http://amdp.phys.strath.ac.uk/tamoc/DATA/RR/>)

⁸ See Curran et al. (2008a) for an inventory of the various masses in a near-by active galaxy.

$$= \frac{4}{3}\pi \alpha_A n_0^2 r_c^3 \left[1 - \frac{r_c^3}{r_c^3 + r_{\text{ion}}^3} \right]. \quad (5)$$

Unlike the Jaffe profile, the photoionisation equilibrium equation can be solved, again giving a ceiling luminosity, albeit less pronounced than for the exponential gas distribution (Fig. 7, top panel). The $L_{\text{UV}} = 10^{23} \text{ W Hz}^{-1}$ threshold of $2.9 \times 10^{56} \lambda \leq 912 \text{ \AA}$ photons per second gives $r_c = 2.6$ kpc, which is very close to the scale-length of the exponential disk and typical of that found for nearby galaxies (de Blok et al. 2008; Oh et al. 2011). For a spherical mass distribution the NFW profile gives

$$\begin{aligned} M_{\text{gas}} &= 4\pi n_0 \int_0^r \frac{r_c/r}{(1 + r/r_c)^2} r^2 dr \\ &= 4\pi n_0 r_c^3 \left[\frac{r_c}{r_c + r} - 1 + \ln(r_c + r) + \ln(r_c) \right], \quad (6) \end{aligned}$$

from which $r_c = 2.6$ kpc gives a total gas mass of $M_{\text{gas}} = 7.1 \times 10^{11} M_{\odot}$, which, not surprisingly given the distribution used, is close to the expected value for the dynamical mass.

The asymptotic density distribution of the NFW profile can be avoided by employing the halo density distribution of an isothermal sphere (Begeman et al. 1991), i.e. $n = n_0/(1 + r/r_c)^2$, Fig. 8 (middle panel). For this, the right hand side of Eq. 1 gives

$$\begin{aligned} 4\pi \alpha_A \int_0^{r_{\text{ion}}} n^2 r^2 &= 4\pi \alpha_A n_0^2 \int_0^{r_{\text{ion}}} \frac{r^2}{(1 + r/r_c)^4} dr \\ &= \frac{4}{3}\pi \alpha_A n_0^2 r_c^3 \left[1 - \frac{r_c(r_c^2 + 3r_c r + 3r^2)}{(r_c + r)^3} \right], \quad (7) \end{aligned}$$

which yields $r_c \approx 3.7$ kpc for $2.9 \times 10^{56} \lambda \leq 912 \text{ \AA}$ photons per second. Note that the ceiling luminosities are more pronounced than for the NFW profile, due to the steeper power law rise at $r < r_c$, similar to that of the exponential gas distribution (Fig. 8, top panel). For a spherical mass distribution the profile gives

$$\begin{aligned} M_{\text{gas}} &= 4\pi n_0 \int_0^r \frac{r^2}{(1 + r/r_c)^2} dr \\ &= 4\pi n_0 r_c^3 \left[1 + \frac{r}{r_c} - \frac{r_c}{r_c + r} - 2 \ln(r_c + r) + 2 \ln(r_c) \right], \quad (8) \end{aligned}$$

which again gives a physically unrealistic total gas mass, $M_{\text{gas}} \approx 9 \times 10^{16} M_{\odot}$.

Based on the derived gas masses, we therefore conclude that the exponential distribution is the most relevant to the density profile of the CNM within the host galaxy, although the alternative models do reproduce the observed critical $\lambda \leq 912 \text{ \AA}$ luminosity for a similar scale-length (all of which, at ≈ 3 kpc, are close to that of the Milky Way). Although the exponential distribution may apply to our own galaxy (Kalberla et al. 2007) and, through the assumption of the canonical values, reproduces the observed critical luminosity and gas mass, currently we do not have the means to map the density profile of the CNM at high redshift. Saying this, the important point is that all of these distributions introduces a critical luminosity above which all of the gas is ionised: At lower radii, when the last term

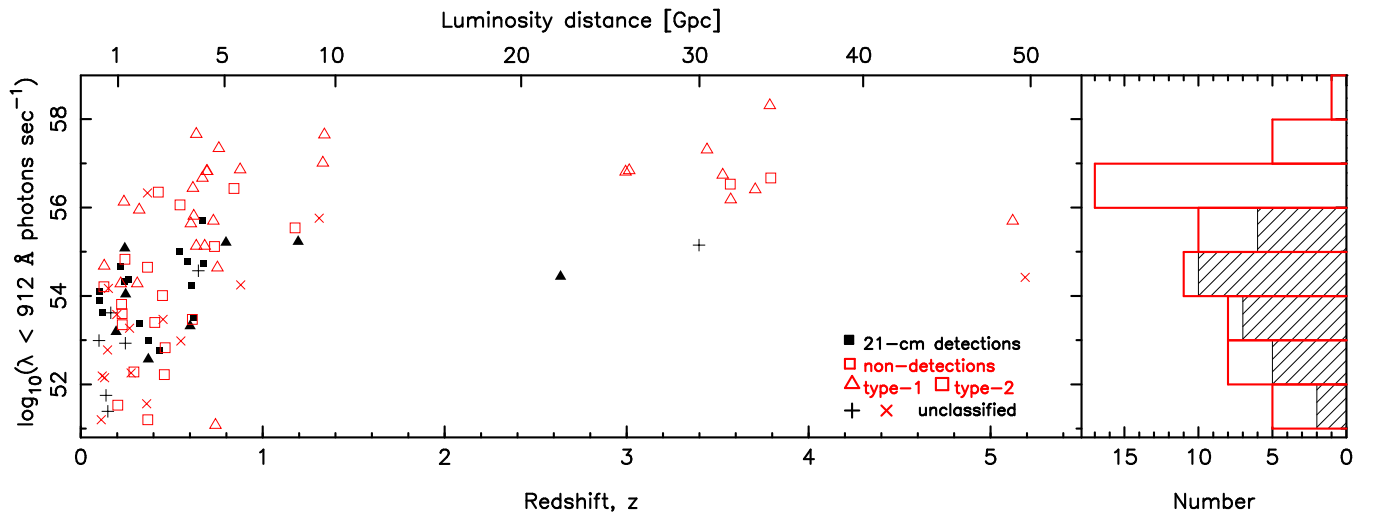


FIG. 4.— The rate of ionising ($\lambda < 912 \text{ \AA}$, bottom) photons versus redshift for the sources searched in 21-cm absorption, obtained from the polynomial fits to the SEDs (Curran et al. 2012). The symbols and histograms are as per Fig. 1.

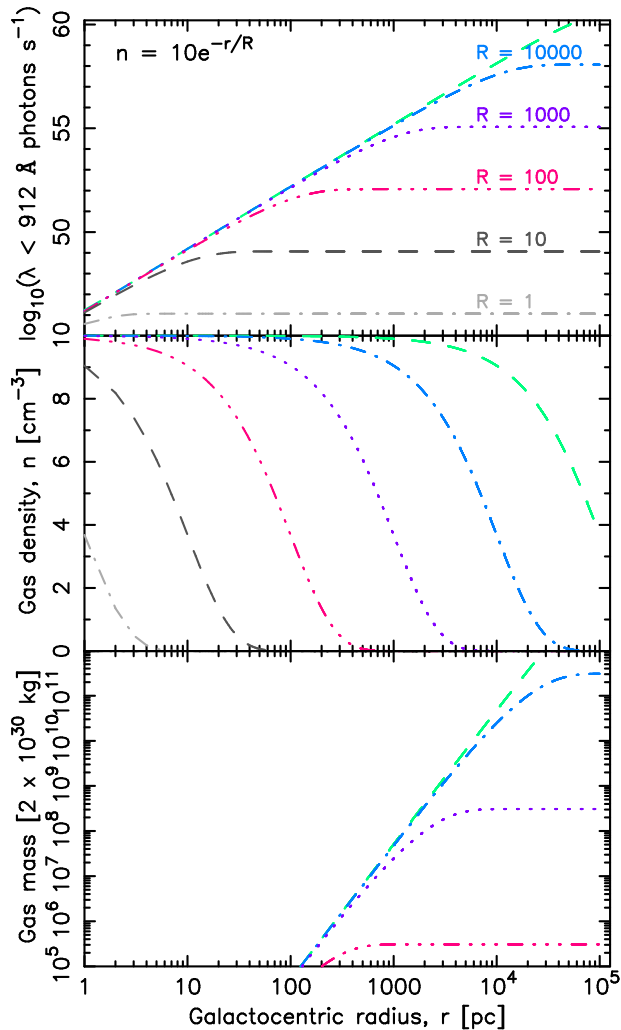


FIG. 5.— The number of ionising ($\lambda < 912 \text{ \AA}$) photons per second (top), particle density (middle) and gas mass in solar masses (bottom) versus the galactocentric radius for an exponential gas distribution at a temperature of 2000 K ($\alpha_A = 1.27 \times 10^{-12} \text{ cm}^3 \text{ sec}^{-1}$). The different line styles represent the various scale-lengths, R , in parsecs, applied to the gas density distribution, $n = n_0 e^{-r/R}$, with the top panel showing the radius of ionised gas for each value of R .

in Eqs. 2, 5 and 7 are important, a power law is seen where $\log_{10} r_{\text{ion}} \propto \log_{10} \int (L_\nu/h\nu) d\nu$, which is the also the case for a constant gas density profile (Osterbrock 1989). However, for a sufficiently high luminosity, this term is negligible and $r_{\text{ion}} \rightarrow \infty$, where the decreasing UV flux with distance from the AGN maintains a sufficient number photons to fully ionise the thinning gas.

3. DISCUSSION AND CONCLUSIONS

From the first high redshift survey of associated 21-cm absorption, Curran et al. (2008b) found an apparent lack of cool neutral gas within the hosts of radio galaxies and quasars. Upon an analysis of the photometry of each source, a strong correlation between the $\lambda = 1216 \text{ \AA}$ continuum luminosity of the AGN and the non-detection of 21-cm was found. Specifically, that 21-cm absorption has never been detected in a source in which the luminosity exceeds $L_{1216} \sim 10^{23} \text{ W Hz}^{-1}$. Although other factors may contribute to the raising of the spin temperature of the gas, the fact that 21-cm cannot be detected above

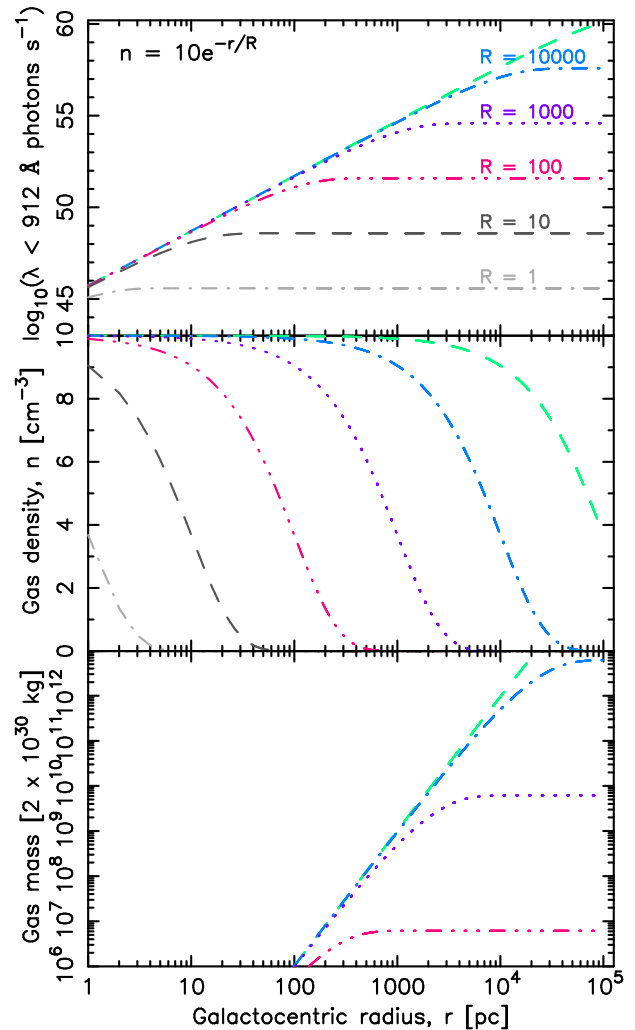


FIG. 6.— As Fig. 5 but for a gas temperature of 10000 K ($\alpha_A = 4.19 \times 10^{-13} \text{ cm}^3 \text{ sec}^{-1}$) and a spherical gas distribution.

the ground state, in conjunction with the lack of detections above this critical luminosity (significant at 4.76σ), strongly suggests that excitation by $\lambda \leq 1216 \text{ \AA}$ photons is the dominant cause of the dearth of 21-cm in optically bright radio sources.

Here we demonstrate that this critical luminosity is also applicable to ionising ($\lambda \leq 912 \text{ \AA}$) photons, showing that associated 21-cm is not detected for any source where $L_{912} \gtrsim 10^{23} \text{ W Hz}^{-1}$ or, more precisely, when there are $\gtrsim 2.9 \times 10^{56}$ ionising photons sec^{-1} . Applying this photoionisation rate, together with various gas density distribution models to the equation of photoionisation equilibrium, from canonical values for the gas density ($n_0 = 10 \text{ cm}^{-3}$) and the recombination rate coefficient ($\alpha_A = 1.27 \times 10^{-12} \text{ cm}^3 \text{ sec}^{-1}$):

- We obtain the observed critical photon rate for a scale-length of $\approx 3 \text{ kpc}$ for all of the tested profiles (exponential, NFW and isothermal sphere). This scale-length is the same as that for the HI in the Milky Way, thus suggesting that the observed critical value is just sufficient to ionise all of the neutral gas within a large spiral galaxy.
- This scale-length gives:

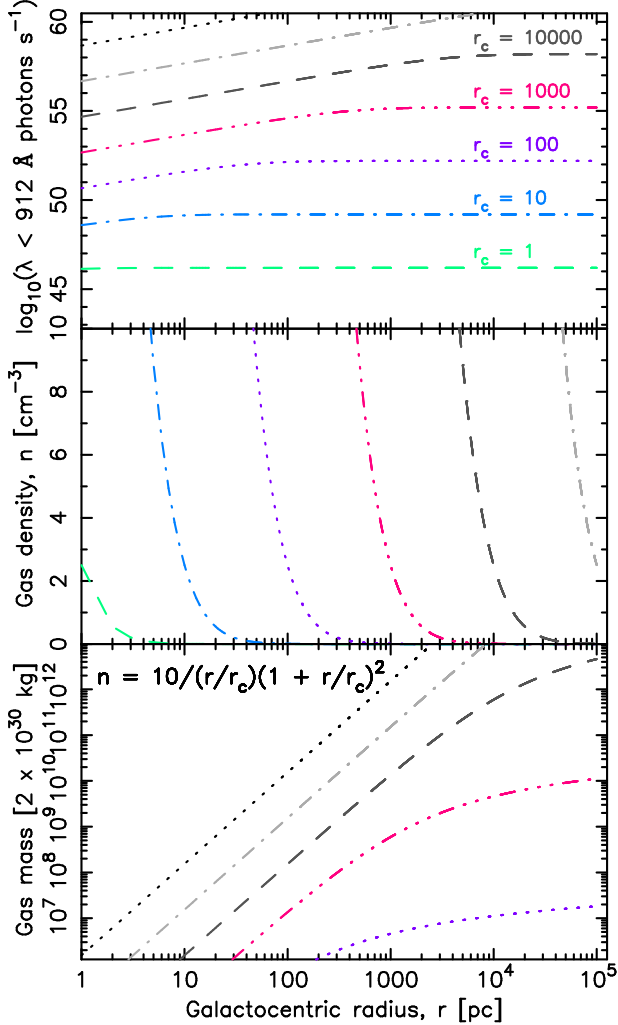


FIG. 7.— As Fig. 5 ($n_0 = 10 \text{ cm}^{-3}$ and $T = 2000 \text{ K}$) but for an NFW profile.

- For an exponential distribution within a disk, a total gas mass of $M_{\text{gas}} = 7.5 \times 10^9 M_{\odot}$, typical of that found from 21-cm emission studies of low redshift galaxies.
- For the NFW and isothermal sphere distributions, a total gas mass which exceeds the total expected dynamical mass of the galaxy.

This leads us to conclude that the exponential profile is the more applicable to the distribution of the CNM (see Kalberla & Kerp 2009), although all of the models give a critical UV luminosity. That is, for a gas profile in which the density decreases with distance from the nucleus, the Strömgen sphere has an infinite radius for a finite luminosity. This suggests that a balance is maintained between the decreasing number of photons and number of particles with increasing distance from the ionising source.

For the sources under consideration here, the critical photon rate (where $L_{912} \sim L_{1216} \sim 10^{23} \text{ W Hz}^{-1}$) is consistent with the dearth of 21-cm detections in all searched high redshift sources (Curran et al. 2008b). A “proximity effect” for highly ionised Lyman- α forest clouds has previously been noted (Weymann et al. 1981; Bajtlik et al. 1988), where in these intervening systems

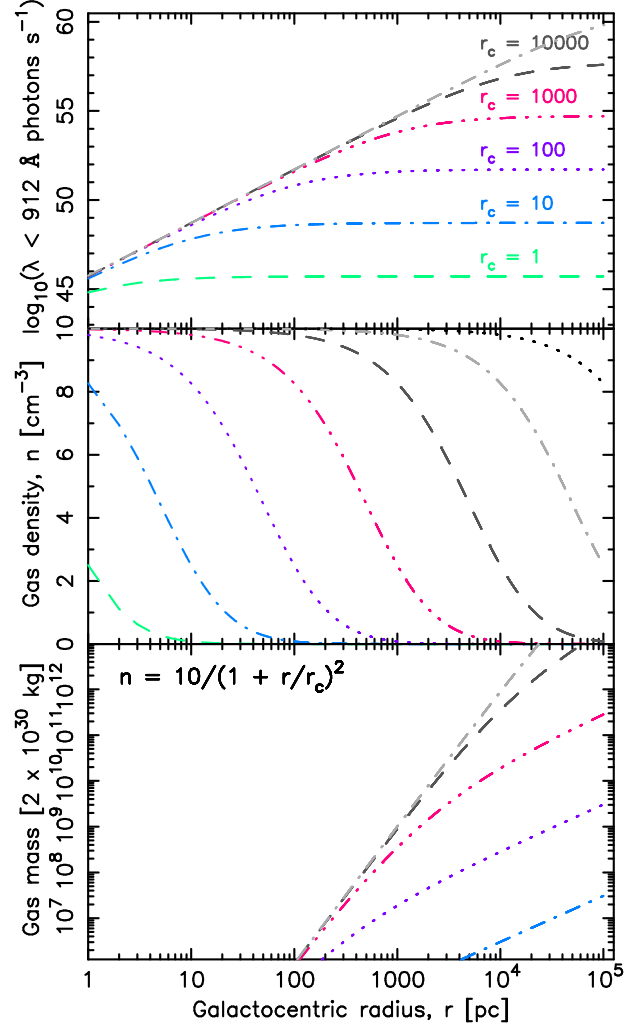


FIG. 8.— As Fig. 7 ($n_0 = 10 \text{ cm}^{-3}$ and $T = 2000 \text{ K}$) but for a halo profile with an isothermal sphere density distribution.

the high ionising flux from the QSO is believed to be responsible for the decrease in the number density of the Lyman- α lines as the redshift of the absorbing galaxy approaches that of the QSO ($z_{\text{abs}} \rightarrow z_{\text{QSO}}$).⁹

However, until our high redshift survey of radio galaxies and quasars, no such effect was known for the 21-cm transition.¹⁰ Furthermore, the 21-cm effect is striking in that, rather than a gradual decrease in associated 21-cm absorption with increasing ultra-violet luminosity, there is an abrupt cut-off in the 21-cm detection rate at a single critical luminosity. We show here that, for a typical spectral energy distribution, this is the luminosity required to completely ionise the large-scale distribution of atomic gas in a large spiral galaxy.¹¹

⁹ Bahcall & Ekers (1969) also show that both the 21-cm and the Lyman- α flux can contribute to higher spin temperatures at absorber–quasar separations of less than a few tens of kpc.

¹⁰ From a study of absorber clustering around QSOs in the SDSS DR3, Wild et al. (2008) suggest that the QSO destroys the Mg II clouds out to beyond 800 kpc. Mg II has an ionisation potential of 15.04 eV, close that of H I (13.60 eV) and so a similar critical $\lambda < 827 \text{ \AA}$ luminosity could perhaps account for this.

¹¹ Although not searched in 21-cm, we derive an ionising photon rate of $3.6 \times 10^{57} \text{ sec}^{-1}$ ($L_{912} = 2.1 \times 10^{24} \text{ W Hz}^{-1}$) for PKS0424–131. Since this is an order of magnitude higher than

There is the possibility that the non-detection of 21-cm absorption in the high-luminosity sample is simply due to orientation effects – as mentioned previously (Sect.1), the majority (17 of 19) of the $L_{UV} \gtrsim 10^{23} \text{ W Hz}^{-1}$ sources are type-1 AGN. In the plane of the torus there may exist large columns of neutral gas, shielded from the radiation (Hennawi & Prochaska 2007). The orientation of these objects could explain their high UV luminosities, however there are also many type-1 objects below $L_{UV} \lesssim 10^{23} \text{ W Hz}^{-1}$, which exhibit a 50% probability of detecting 21-cm absorption. This suggests that the absorbing gas is located in the large-scale disk, which must be randomly oriented with respect to the torus (Schmitt et al. 1997; Nagar & Wilson 1999; Curran & Whiting 2010; Lawrence & Elvis 2010).

Therefore, if the non-detection of absorption in the $L_{UV} \gtrsim 10^{23} \text{ W Hz}^{-1}$ sources is due to line-of-sight effects, these differ from the lower luminosity AGN in that, unlike these, the large-scale absorbing disk is always aligned with the obscuring torus. It is possible that for these, the high UV luminosities are indeed the consequence of a direct view to the AGN unobscured by the large-scale disk. This would also explain the lower luminosity type-1 objects in which 21-cm is detected, in that the absorbing gas attenuates the radiation.

Using the orientation as the sole explanation for the differences in absorption rates can not, however, explain why there is a critical value in the UV luminosities rather than a gradual decrease in absorption rates as the luminosity increases. The model presented here naturally yields a critical luminosity, and we have shown that this value is sufficient to ionise all of the CNM in a large spiral galaxy.

Our model is supported by the observation of greatly-decreased $250\mu\text{m}$ emission from AGN above a critical luminosity (Page et al. 2012). The emission is not restricted to the line-of-sight to the nucleus, indicating that the entire galaxy is affected by the presence of a luminous AGN.

Finding redshifted 21-cm absorption is a major science goal of the Square Kilometre Array (SKA). The results found here suggest that the lack of cool neutral gas is not due to a sensitivity issue with current radio telescopes, but a real effect caused by the presence of a quasar in a galaxy of gas. That is, *the known high redshift radio galaxies and quasars are probably devoid of a large-scale distribution of neutral gas.*¹² This neutral gas provides the fuel for star formation, and our result suggests that the AGN could therefore suppress star formation in the large-scale disk. Note also that, although the $250 \mu\text{m}$ fluxes are also subject to a sensitivity limit, the deficit of $250 \mu\text{m}$ above a critical luminosity is further evidence of a suppression of star formation (Page et al. 2012). Here we show that this is not a sensitivity issue, but that the neutral gas, and most likely, appreciable star formation activity is simply not present.

Therefore, even the SKA will be unlikely to find this cool gas in the objects currently known. Where it will excel, however, is in blind surveys of radio sources from which the visible light is too faint to be detected by optical instruments (Curran et al. 2009). Although unseen, these sources must exist in order to have had star formation within the host galaxies of early AGN. As such, the traditional optical selection of targets must be abandoned in order to find the missing star-forming material within high redshift radio sources.

We would like to thank John Webb, Bob Carswell, Elliot Koch, Julian Berengut, Catherine Greenhill and Nigel Badnell for their helpful input and advice. This research has made use of the NASA/IPAC Extragalactic Database (NED) which is operated by the Jet Propulsion Laboratory, California Institute of Technology, under contract with the National Aeronautics and Space Administration. This research has also made use of NASA’s Astrophysics Data System Bibliographic Service. The Centre for All-sky Astrophysics is an Australian Research Council Centre of Excellence, funded by grant CE110001020.

REFERENCES

- Allison, J. R., Curran, S. J., Emonts, B. H. C., et al. 2012, MNRAS, 423, 2601
- Athreya, R. M., Kapahi, V. K., McCarthy, P. J., & van Breugel, W. 1998, A&A, 329, 809
- the critical rate, it could account for “the mysterious absence of neutral hydrogen”, as traced by Lyman- α emission, close to this source (Francis & Bland-Hawthorn 2004). Bruns et al. (2012) also suggest that the UV emission could be responsible, thus suppressing the star formation.
- ¹² Simulations suggest that, while the HI content in galaxies is similar to present day values, the molecular component (H_2) is larger at $z \gtrsim 1$ (Obreschkow & Rawlings 2009). For gas densities typical of molecular clouds, $n_0 \sim 1000 \text{ cm}^{-3}$, the critical ionising photon flux of $2.9 \times 10^{56} \text{ sec}^{-1}$ gives a scale-length of $\approx 100 \text{ pc}$ at 2000 K, or $\approx 50 \text{ pc}$ at a more realistic 20 K. Conversely, luminosities of $L_{912} \approx 2 \times 10^{27} \text{ W Hz}^{-1}$ (3×10^{60} photons sec^{-1}) and $4 \times 10^{28} \text{ W Hz}^{-1}$ (5×10^{61} photons sec^{-1}) are required to fully ionise a CNM with $n_0 \sim 1000 \text{ cm}^{-3}$ with a scale-length of 3 kpc at 2000 and 20 K, respectively. If the deficit of neutral gas at high redshift was due to the gas being mostly molecular, there would be little reason for a lack of 21-cm to be correlated with the $\lambda = 912 \text{ \AA}$ luminosity (although a lack of H_2 could be). In any case, the HI deficit is observed at all redshifts, as well as there being no observational evidence for a high molecular gas content within the hosts of radio galaxies and quasars (Curran et al. 2011b).
- Bahcall, J. N. & Ekers, R. D. 1969, ApJ, 157, 1055
- Bajtlík, S., Duncan, R. C., & Ostriker, J. P. 1988, ApJ, 327, 570
- Begeman, K. G., Broeils, A. H., & Sanders, R. H. 1991, MNRAS, 249, 523
- Bruns, Jr., L. R., Wyithe, J. S. B., Bland-Hawthorn, J., & Dijkstra, M. 2012, MNRAS, 2543, 421
- Catinella, B., Haynes, M. P., Giovanelli, R., Gardner, J. P., & Connolly, A. J. 2008, ApJ, 685, L13
- Curran, S. J. 2010, MNRAS, 402, 2657
- , 2012, ApJ, 748, L18
- Curran, S. J., Koribalski, B. S., & Bains, I. 2008a, MNRAS, 389, 63
- Curran, S. J., Tzanavaris, P., Darling, J. K., et al. 2010, MNRAS, 402, 35
- Curran, S. J. & Webb, J. K. 2006, MNRAS, 371, 356
- Curran, S. J., Webb, J. K., Murphy, M. T., et al. 2002, PASA, 19, 455
- Curran, S. J., Whiting, M. T., Murphy, M. T., et al. 2011a, MNRAS, 413, 1165
- Curran, S. J. & Whiting, M. T. 2010, ApJ, 712, 303
- Curran, S. J., Whiting, M. T., Combes, F., et al. 2011b, MNRAS, 416, 2143
- Curran, S. J., Whiting, M. T., Sadler, E. M., & Bignell, C. 2012, MNRAS, in press (arXiv:1210.1886)
- Curran, S. J., Whiting, M. T., Tanna, A., Bignell, C., & Webb, J. K. 2011c, MNRAS, 413, L86

- Curran, S. J., Whiting, M. T., & Webb, J. K. 2009, *Proceedings of Science*, 89, Chap. 11
- Curran, S. J., Whiting, M. T., Webb, J. K., & Athreya, A. 2011d, *MNRAS*, 414, L26
- Curran, S. J., Whiting, M. T., Wiklind, T., et al. 2008b, *MNRAS*, 391, 765
- de Blok, W. J. G., Walter, F., Brinks, E., et al. 2008, *AJ*, 136, 2648
- Draine, B. T. 2011, *Physics of the Interstellar and Intergalactic Medium* (Princeton University Press)
- Field, G. B. 1959, *ApJ*, 129, 536
- Francis, P. J. & Bland-Hawthorn, J. 2004, *MNRAS*, 353, 301
- Gopal-Krishna & Wiita, P. J. 2000, *ApJ*, 529, 189
- Grasha, K. & Darling, J. 2011, in *American Astronomical Society Meeting Abstracts*, Vol. 43, 345.02
- Gupta, N., Salter, C. J., Saikia, D. J., Ghosh, T., & Jeyakumar, S. 2006, *MNRAS*, 373, 972
- Haiman, Z. & Rees, M. J. 2001, *ApJ*, 556, 87
- Hennawi, J. F. & Prochaska, J. X. 2007, *ApJ*, 655, 735
- Jaffe, W. 1983, *MNRAS*, 202, 995
- Kalberla, P. M. W., Dedes, L., Kerp, J., & Haud, U. 2007, *A&A*, 469, 511
- Kalberla, P. M. W. & Kerp, J. 2009, *Ann. Rev. Astr. Ap.*, 47, 27
- Koribalski, B. S., Staveley-Smith, L., Kilborn, V. A., et al. 2004, *AJ*, 128, 16
- Lawrence, A. & Elvis, M. 2010, *ApJ*, 714, 561
- Martin, C., Barlow, T., Barnhart, W., et al. 2003, in *Society of Photo-Optical Instrumentation Engineers (SPIE) Conference Series*, Vol. 4854, *Society of Photo-Optical Instrumentation Engineers (SPIE) Conference Series*, ed. J. C. Blades & O. H. W. Siegmund, 336–350
- Morganti, R., Oosterloo, T. A., Tadhunter, C. N., et al. 2001, *MNRAS*, 323, 331
- Nagar, N. M. & Wilson, A. S. 1999, *ApJ*, 516, 97
- Navarro, J. F., Frenk, C. S., & White, S. D. M. 1996, *ApJ*, 462, 563
- Noterdaeme, P., Petitjean, P., Ledoux, C., & Srianand, R. 2009, *A&A*, 505, 1087
- Obreschkow, D. & Rawlings, S. 2009, *ApJ*, 696, L129
- Oh, S.-H., de Blok, W. J. G., Brinks, E., Walter, F., & Kennicutt, Jr., R. C. 2011, *AJ*, 141, 193
- Osterbrock, D. E. 1989, *Astrophysics of Gaseous Nebulae and Active Galactic Nuclei* (Mill Valley, California: University Science Books)
- Osterbrock, D. E. & Ferland, G. J. 2006, *Astrophysics of gaseous nebulae and active galactic nuclei* (Sausalito, California: University Science Books)
- Page, M. J., Symeonidis, M., Vieira, J. D., et al. 2012, *Nature*, 485, 213
- Péroux, C., Storrie-Lombardi, L. J., McMahon, R. G., Irwin, M., & Hook, I. M. 2001, *AJ*, 121, 1799
- Pihlström, Y. M., Conway, J. E., & Vermeulen, R. C. 2003, *A&A*, 404, 871
- Purcell, E. M. & Field, G. B. 1956, *ApJ*, 124, 542
- Schlegel, D. J., Finkbeiner, D. P., & Davis, M. 1998, *ApJ*, 500, 525
- Schmitt, H. R., Kinney, A. L., Storchi-Bergmann, T., & Antonucci, R. 1997, *ApJ*, 477, 623
- Scott, J. E., Kriss, G. A., Brotherton, M., et al. 2004, *ApJ*, 615, 135
- Shull, J. M., Stevans, M., & Danforth, C. W. 2012, *ApJ*, 752, 162
- Srianand, R., Gupta, N., Petitjean, P., Noterdaeme, P., & Ledoux, C. 2010, *MNRAS*, 401, 1888
- Taylor, G. L., Dunlop, J. S., Hughes, D. H., & Robson, E. I. 1996, *MNRAS*, 283, 930
- Telfer, R. C., Zheng, W., Kriss, G. A., & Davidsen, A. F. 2002, *ApJ*, 565, 773
- Uson, J. M., Bagri, D. S., & Cornwell, T. J. 1991, *PhRvL*, 67, 3328
- Weymann, R. J., Carswell, R. F., & Smith, M. G. 1981, *ARA&A*, 19, 41
- Wild, V., Kauffmann, G., White, S., et al. 2008, *MNRAS*, 388, 227
- Wolfe, A. M. & Burbidge, G. R. 1975, *ApJ*, 200, 548